

Electronic Supplementary Information

A Polydopamine-Based Biomimetic Multifunctional Nanoplatfom for Multilayer Imaging of Cancer Biomarkers Carried by Extracellular Vesicles

Ze-Rui Zhou, Xiao-Yuan Wang, Jian Lv and Ruo-Can Qian*

Key Laboratory for Advanced Materials & School of Chemistry and Molecular Engineering, East China
University of Science and Technology, Shanghai 200237, P. R. China

E-mail: ruocanqian@ecust.edu.cn

Table of Contents

Supplementary Note 1. Characterization of GNP Core Solution	5
Figure S1. UV-vis absorbance spectra of a) bare GNPs, b) GNP@PDA and c) GNP@PDA-NP. d) TEM image of the 60 nm GNPs (scale bar: 100 nm).	
Supplementary Note 2. Size Distribution of GNP, GNP@PDA and GNP@PDA-NP	6
Figure S2. TEM images and size distribution of a) bare GNPs, b) GNP@PDA and c) GNP@PDA-NP. d) Statistical analysis of nanoparticle size by Image J (scale bar: 100 nm).	
Supplementary Note 3. SA Induced Fluorescence Recovery of DAPB	7
Figure S3. Average blue fluorescence intensity of GNP@PDA-NP solution and the mixture of GNP@PDA-NP and SA before and after 60 min incubation.	
Supplementary Note 4. MiRNA-21 Triggered Fluorescence Recovery of MB	8
Figure S4. Average green fluorescence intensity of GNP@PDA-NP solution and the mixture of GNP@PDA-NP and miRNA-21 before and after 60 min incubation.	
Supplementary Note 5. Specific Recognition Between SA and DAPB	9
Figure S5. Average blue fluorescence intensity of GNP@PDA-NP solution and the mixture of GNP@PDA-NP and mannose before and after 60 min incubation.	
Supplementary Note 6. Specific Recognition Between MiRNA-21 and MB	10
Figure S6. Average green fluorescence intensity of GNP@PDA-NP solution and the mixture of GNP@PDA-NP and mismatched miRNA-21 before and after 60 min incubation.	
Supplementary Note 7. Stability of GNP@PDA-NP in Various Medium	11

Figure S7. UV-vis characterization of GNP@PDA-NP in 1640 cell medium (10% FBS) and DMEM cell medium (10% FBS) before and after 24 h incubation.

Figure S8. Average green and blue fluorescence intensity of GNP@PDA-NP in 1640 cell medium (10% FBS) and DMEM cell medium (10% FBS) before and after 24 h incubation.

Supplementary Note 8. Fabrication of EV Detection Surface on 96-Well Plates **12**

Figure S9. SEM images (scale bar: 200 nm) and dark field images (scale bar: 2 μ m) of a) bare GNPs, b) GNP@PDA and c) GNP@PDA-NP.

Supplementary Note 9. Detection of the miRNA-21 Concentration in EVs by qRT-PCR **13-16**

Figure S10. MiRNA-21 in HeLa EVs detected by qRT-PCR. a) The table showing the qRT-PCR data. b) Amplification curve and solubility curve. c) Canonical plotting.

Supplementary Note 10. The Detection of EVs by Western Blot and Immunofluorescence Labeling **16-17**

Figure S11. Western blot analysis of the surface markers (CD81 and CD63) in EV samples.

Figure S12. Microscopic images of EV surface markers (left: CD81, right: CD63) marked by immunofluorescence antibodies.

Supplementary Note 11. Optimization of the Fabrication on 96-Well Plates **18**

Figure S13. Microscopic images of EVs derived from HeLa cells (200 μ L HeLa supernatant was added to each well and incubated for different time, add 100 μ L the mixed solution, with laser irradiation for 30min, standing for 30 min before microscopic imaging) (scale bar: 30 μ m).

Supplementary Note 12. Photothermal Effect of GNP@PDA-NPs **19-21**

Figure S14. a) Gold particle photothermal effect diagram. b) Microscopic images of EVs derived from HeLa cells (200 μ L HeLa supernatant was treated with laser irradiation without GNP@PDA-NPs for 30 min before microscopic imaging) (scale bar: 30 μ m).

Supplementary Note 13. Fluorescence Distribution of the EVs with Different Sizes **22**

Figure S15. Blue/green channel distribution of the EVs of different sizes from different cells (60 EVs for each cell type, 20 EVs for each size).

Supplementary Note 14. Size Distribution of EVs Derived from Cells Treated with Drugs **23**

Figure S16. Pie charts showing the average size distribution of EVs derived from HeLa cells treated with a) control, b) anti-miRNA-21 (200 nM), c) SD (60 mU), d) anti-miRNA-21 (200 nM) + SD (60 mU).

Supplementary Note 15. Size Distribution of the EVs from Serum Samples **24**

Figure S17. Pie charts showing the average size distribution of EVs in serum samples taken from healthy controls and HCC patients.

Supplementary Note 1. Characterization of GNP Core Solution

As the concentration of the GNP solution is proportional to the absorption, the concentrated GNP solution was characterized by UV-Vis spectra. From the absorption peak, the concentration of GNP solution was calculated to be 0.014 nM.¹

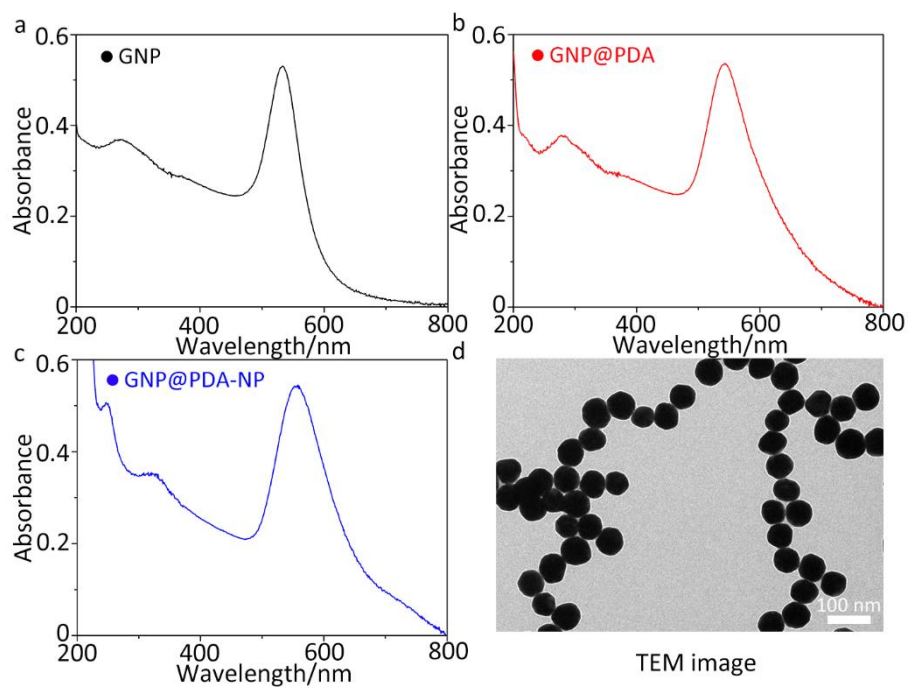


Figure S1. UV-vis absorbance spectra of a) bare GNPs, b) GNP@PDA and c) GNP@PDA-NP. d) TEM image of the 60 nm GNPs (scale bar: 100 nm).

Supplementary Note 2. Size Distribution of GNP, GNP@PDA and GNP@PDA-NP

GNP, GNP@PDA and GNP@PDA-NP were characterized by TEM. Size distribution was counted from the TEM images by Image J.

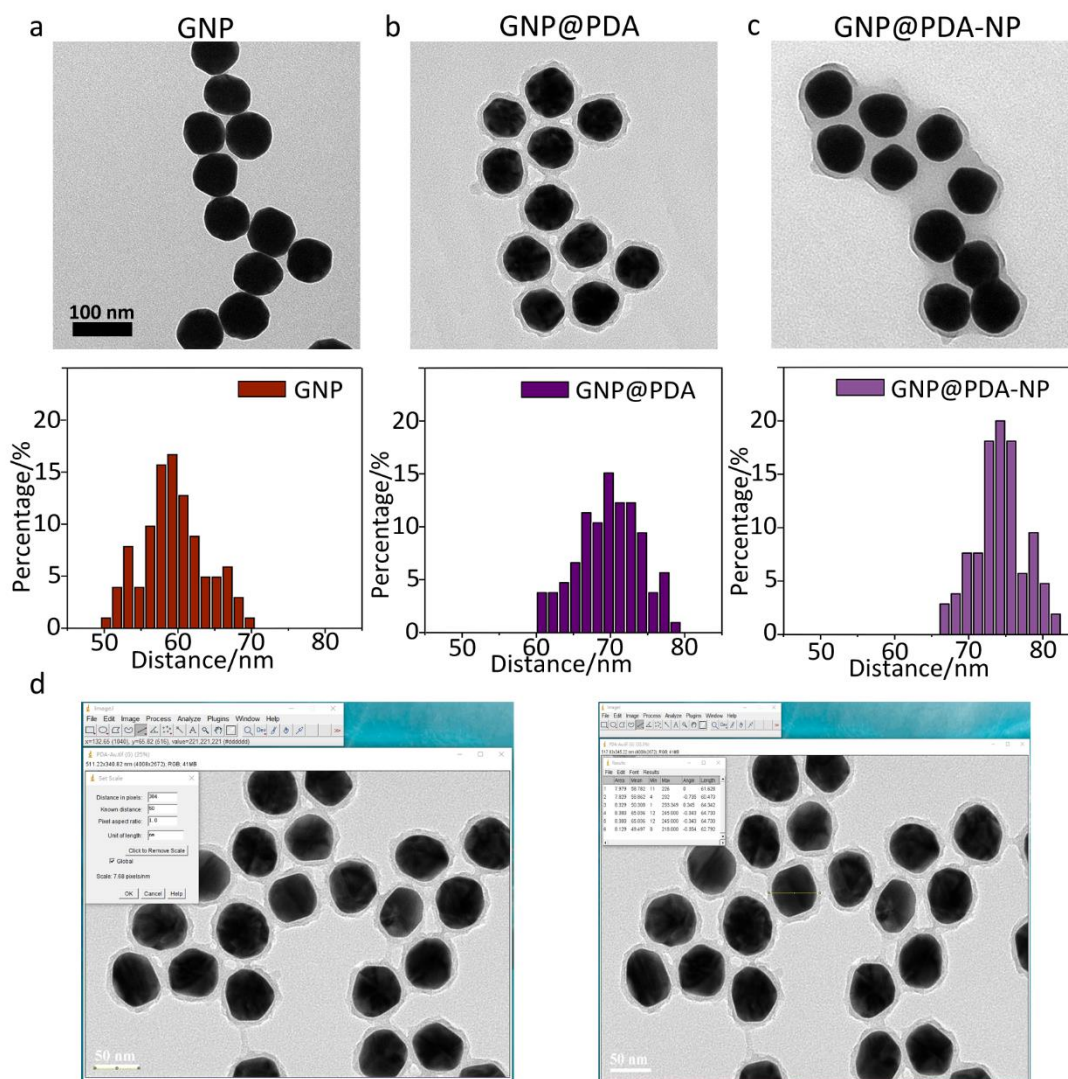


Figure S2. TEM images and size distribution of a) bare GNPs, b) GNP@PDA and c) GNP@PDA-NP. d) Statistical analysis of nanoparticle size by Image J (scale bar: 100 nm).

Supplementary Note 3. SA Induced Fluorescence Recovery of DAPB

GNP@PDA-NP solution (0.014 nM) was treated with SA (100 nM) and the fluorescence of the mixture was observed (ex: 340 nm, em: 490 nm). GNP@PDA-NP responded quickly to SA treatment within 60 min, indicating the blue fluorescence recovery of DAPB induced by the combination of SA and DAPB.

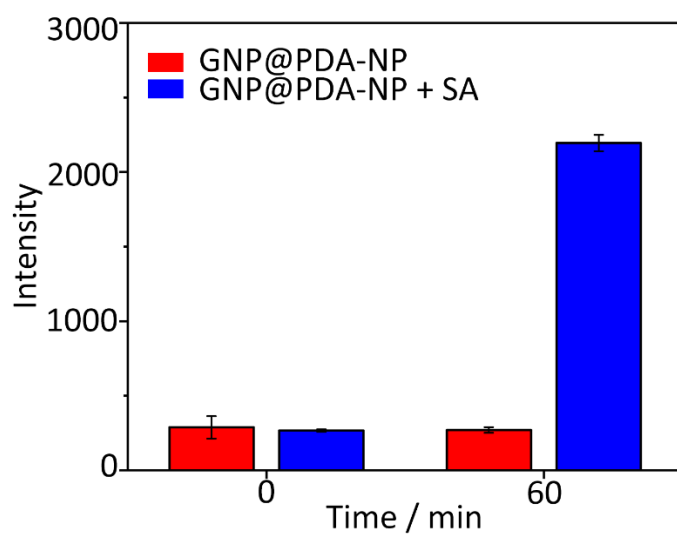


Figure S3. Average blue fluorescence intensity of GNP@PDA-NP solution and the mixture of GNP@PDA-NP and SA before and after 60 min incubation.

Supplementary Note 4. MiRNA-21 Triggered Fluorescence Recovery of MB

The GNP@PDA-NP solution (0.014 nM) was treated with miRNA-21 (100 nM) and the fluorescence of the mixture was observed (ex: 500 nm, em: 570 nm). GNP@PDA-NP responded quickly to miRNA-21 treatment within 60 min, indicating the green fluorescence recovery of Cy3 triggered by the miRNA-21 induced MB hairpin opening and departure.

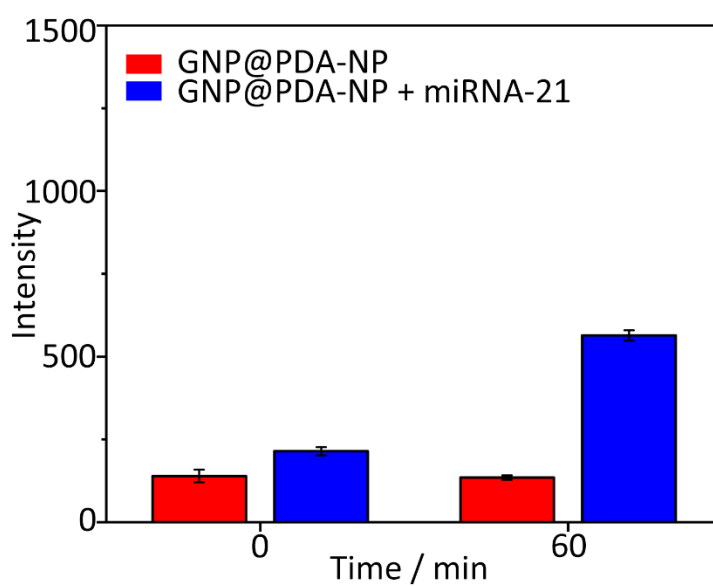


Figure S4. Average green fluorescence intensity of GNP@PDA-NP solution and the mixture of GNP@PDA-NP and miRNA-21 before and after 60 min incubation.

Supplementary Note 5. Specific Recognition Between SA and DAPB

To demonstrate the specific combination between SA and DAPB on the surface of GNP@PDA-NP, mannose (100 nM) was used instead of SA to mix with the GNP@PDA-NP solution (0.014 nM), and then the fluorescence of the mixture was observed (ex: 340 nm, em: 490 nm). No obvious changes in fluorescence intensity were observed over time, indicating the specific binding between SA and DAPB.

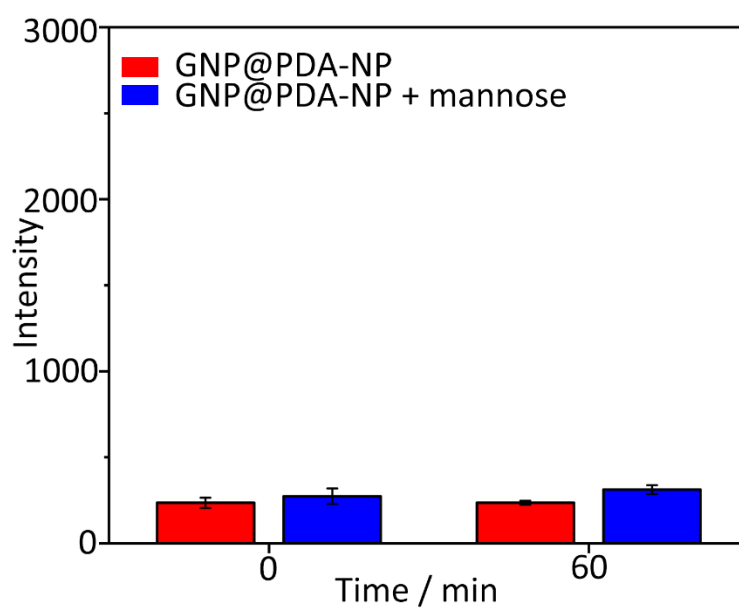


Figure S5. Average blue fluorescence intensity of GNP@PDA-NP solution and the mixture of GNP@PDA-NP and mannose before and after 60 min incubation.

Supplementary Note 6. Specific Recognition Between MiRNA-21 and MB

To demonstrate the specific combination between miRNA-21 and MB on the surface of GNP@PDA-NP, mismatched miRNA-21 (100 nM) was used instead of miRNA-21 to mix with the GNP@PDA-NP solution (0.014 nM), and then the fluorescence of the mixture was observed (ex: 500 nm, em: 570 nm). No obvious changes in fluorescence intensity were observed over time, indicating the specific binding between miRNA-21 and MB.

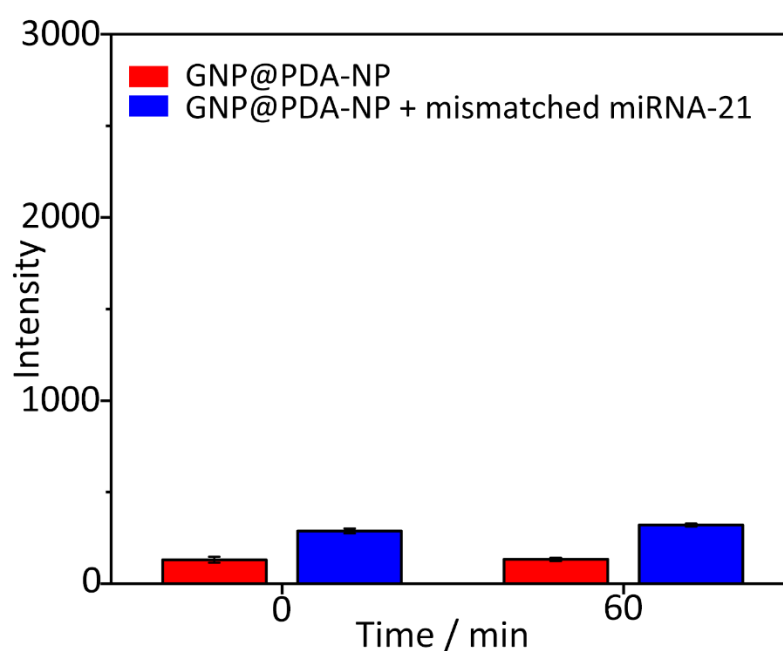


Figure S6. Average green fluorescence intensity of GNP@PDA-NP solution and the mixture of GNP@PDA-NP and mismatched miRNA-21 before and after 60 min incubation.

Supplementary Note 7. Stability of GNP@PDA-NP in Various Medium

The GNP@PDA-NP solution (200 μ L each) was mixed with 200 μ L different cell culture medium (1640, DMEM) containing 10% FBS, and incubated at 37 $^{\circ}$ C for 24 h. The mixture was sent for UV-vis analysis (Figure S7) and fluorescence detection (Figure S8, ex: 340 nm, em: 490 nm; ex: 500 nm, emission: 570 nm). No obvious changes were observed, indicating good stability of GNP@PDA-NP.

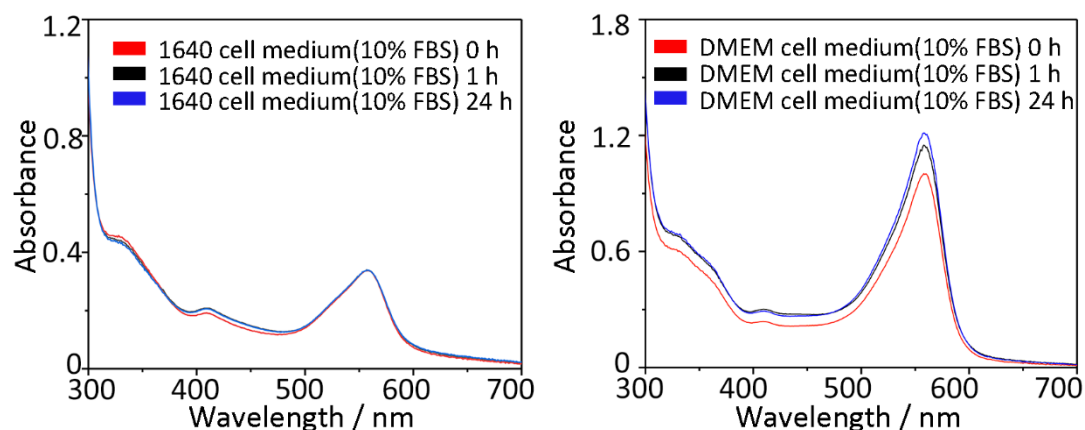


Figure S7. UV-vis characterization of GNP@PDA-NP in 1640 cell medium (10% FBS) and DMEM cell medium (10% FBS) before and after 24 h incubation.

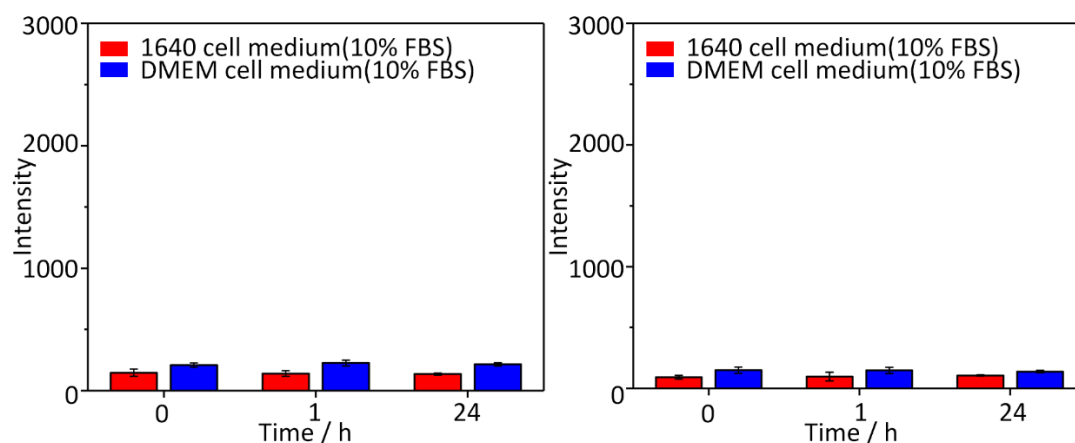


Figure S8. Average green and blue fluorescence intensity of GNP@PDA-NP in 1640 cell medium (10% FBS) and DMEM cell medium (10% FBS) before and after 24 h incubation.

Supplementary Note 8. Fabrication of EV Detection Surface on 96-Well Plates

To realize the combination of GNP@PDA-NP with 96-well plates for high throughput detection, the GNPs were doped in a thin PDA layer on the board, and then functionalized with DAPB, MB and montanic acid. The step-by-step fabrication was characterized by SEM and dark field microscopy.

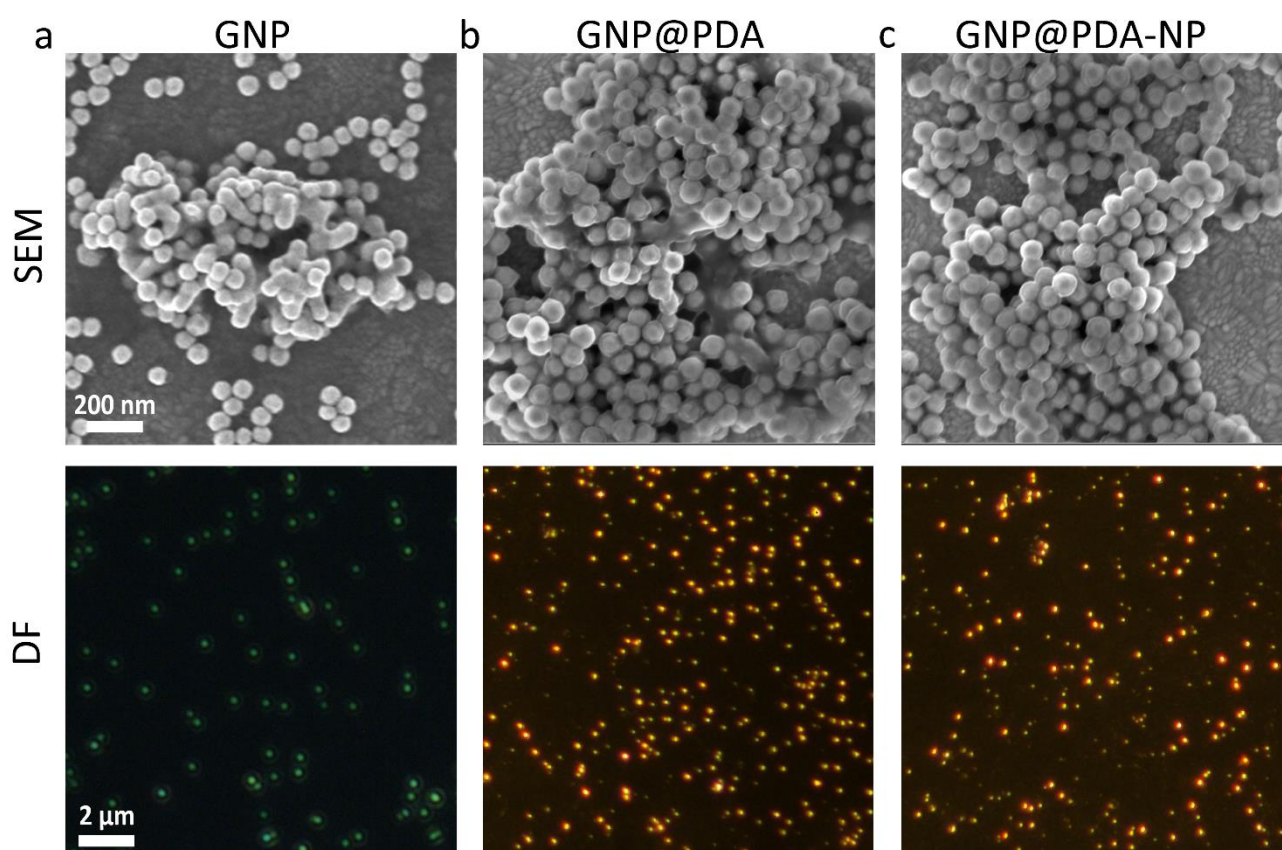


Figure S9. SEM images (scale bar: 200 nm) and dark field images (scale bar: 2 μ m) of a) bare GNPs, b) GNP@PDA and c) GNP@PDA-NP.

Supplementary Note 9. Detection of the miRNA-21 Concentration in EVs by qRT-PCR.

To realize the quantitative evaluation of miRNA-21 in EVs, EVs were isolated from HeLa cell supernatant for miRNA extraction. Total miRNA-21 was isolated from EVs using the TRIzol reagent (Invitrogen), according to manufacturer's instructions. The extracted miRNA-21 was reverse-transcribed using SYBR Premix Ex Taq™ II (TaKaRa), and subjected to qRT-PCR. The PCR program started with an initial heating step at 95 °C for 1 minutes, followed by 40 cycles of denaturation at 95 °C for 15 s and annealing at 60 °C for 30 s. At the end of each cycle, a DNA melting curve of the amplified products was created between 60 °C and 95 °C (readings were taken at 0.1 °C increments) to evaluate the melting temperature (T_m). All samples were tested in triplicate. Using the same reaction conditions as the SYBR Green assay described above, the standard curve was generated using the synthetic miRNA-21 (standard sample), which was assembled from synthetic oligonucleotides. The synthetic miRNA-21 was dissolved in RNase-free distilled water according to the manufacturer's instructions and serially diluted from 0.001 nM to 10000 nM. After the standard curve was obtained, miRNA-21 isolated from EVs were diluted for 10 times before detection. The equation that describes the exponential amplification of PCR is

$$X_n = X_0 * (1 + E_n)^n \quad [1]$$

where X_n is the number of target molecules at cycle n of the reaction, X₀ is the initial number of target molecules. E_n is the efficiency of target amplification, and n is the number of cycles. The threshold cycle (C_T) indicates the fractional cycle number at which the amount of amplified target reaches a fixed threshold. Thus,

$$X_{C_T} = X_0 * (1 + E_n)^{C_T} = M \quad [2]$$

where X_{C_T} is the threshold number of target molecules, C_T is the threshold cycle for target amplification, and M is a constant. The calculation of the miRNA copy number in the sample is based on the measured Ct value and the equation of the calibration range according to the following formula:

$$\lg M = \lg X_0 * (1 + E_n)^{C_T} \quad [3]$$

Therefore,

$$\lg X_0 = \lg M - C_T \lg(1 + E_n) \quad [4]$$

According to the experimental data, the standard curve was shown in **Figure S10 c**, and the equation is as following:

$$Ct = -3.601 \log X_0 + 22.739$$

The PCR results showed that the miRNA-21 concentration in HeLa cell supernatant was 300 nM. Considering that $10^9 \sim 10^{10}$ EVs can be extracted from 1 mL cell supernatant, one vesicle contains $10^4 \sim 10^5$ miRNA-21 molecules. Therefore, the local concentration of miRNA in a single vesicle is sufficient to be detected by fluorescent imaging with our method, as EVs can be effectively enriched and captured by PDA detection surface.

Sample	Target Gene	CT	Average.CTCConcentration(nM)	Finally concentration(nM)	
sd1	hsa-miR-21a-5p	8.909	8.820	10000.000	1.000E+04
		8.765			
		8.786			
sd2	hsa-miR-21a-5p	11.925	11.936	1000.000	1.000E+03
		11.996			
		11.887			
sd3	hsa-miR-21a-5p	15.200	15.211	100.000	1.000E+02
		15.199			
		15.232			
sd4	hsa-miR-21a-5p	18.868	18.860	10.000	1.000E+01
		18.893			
		18.819			
sd5	hsa-miR-21a-5p	22.571	22.580	1.000	1.000E+00
		22.555			
		22.613			
sd6	hsa-miR-21a-5p	26.432	26.385	0.100	1.000E-01
		26.347			
		26.377			
sd7	hsa-miR-21a-5p	29.616	29.689	0.010	1.000E-02
		29.713			
		29.739			
sd8	hsa-miR-21a-5p	33.963	34.027	0.001	1.000E-03
		34.159			
		33.958			
Hela Exo	hsa-miR-21a-5p	17.519	17.463	28.165	292.066
		17.421	17.463	29.978	
		17.448	17.463	29.476	

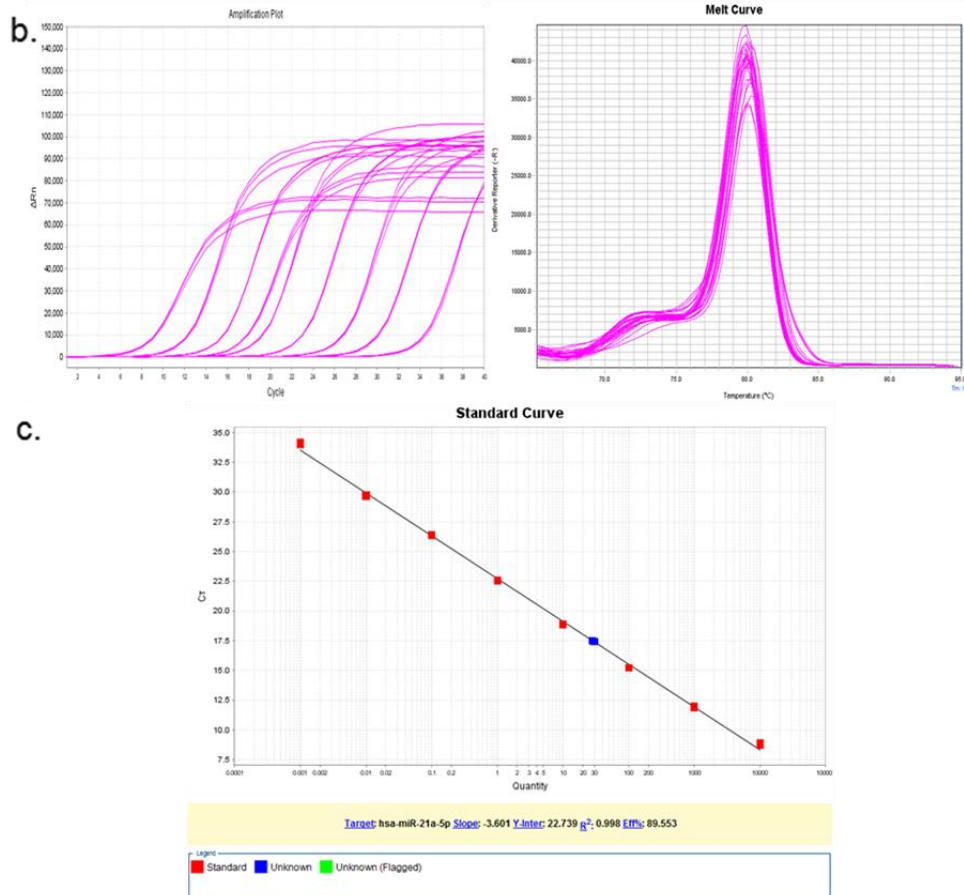


Figure S10. MiRNA-21 in HeLa EVs detected by qRT-PCR. a) The table showing the qRT-PCR data. b) Amplification curve and solubility curve. c) Canonical plotting.

Supplementary Note 10. The Detection of EVs by Western Blot and Immunofluorescence

Labeling

To identify the specific proteins expressed on the membranes of EVs, the purified vesicles derived from the culture medium of HeLa cells were measured by western blot analysis. EVs harvested from HeLa cells were lysed and proteins were obtained by centrifugations. The proteins separated from EVs were subjected to SDS-PAGE. After separation, remove upper side of sample wells with a razor blade. Notching bottom right-hand corner of gel for orientation and put gel in transfer buffer until ready to use. Then the PVDF membrane (Millipore Immobion-P #IPVH 000 10) were prepared according to the size of gel. Afterwards, the proteins were transferred into PVDF membranes (Millipore Immobion-P #IPVH 000 10) by attaching the electrodes, and processed by blocking and immunoreaction. The expression of the common exosomal markers CD63 and CD81 were determined using rabbit polyclonal anti-CD63 antibody and rabbit monoclonal anti-CD81 antibody. Afterwards, the PVDF membranes were imaged and analyzed using FR-1800 Luminescent and fluorescent biological image analysis system. Densitometric analysis was used to calculate the differences in the fold induction of protein levels which were normalized to CD63 or CD81 content. Values were reported as relative amounts. In addition, the immunofluorescence labeling experiments based on a sandwich enzyme-immunoassay protocol were performed, confirming the existence of exosomal marker proteins, CD63 and CD81 (Figure S13). HeLa cells were cultured 3 days and then the medium was sucked out and centrifuged at 5000 rpm for 3 min. The supernatant was then added onto EV detection surface for 30 min. Afterwards, the captured EVs were treated with anti-CD63 antibody [MEM-259] or anti-CD81 antibody [M38] for 30 min respectively. Afterwards, the EVs were stained with Alexa Fluor 488-conjugated AffiniPure Goat Anti-Rabbit IgG (H+L) or Alexa Fluor 594-conjugated AffiniPure Goat Anti-Rabbit IgG (H+L) for 30 min respectively following the manufacturer's instruction. The immunofluorescence labeled samples were washed with PBS and then observed under fluorescence microscope.

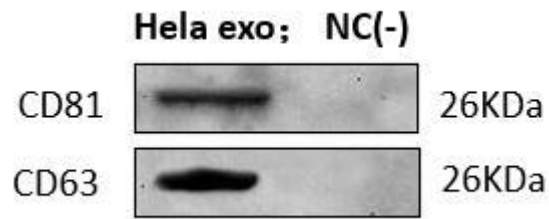


Figure S11. Western blot analysis of the surface markers (CD81 and CD63) in EV samples.

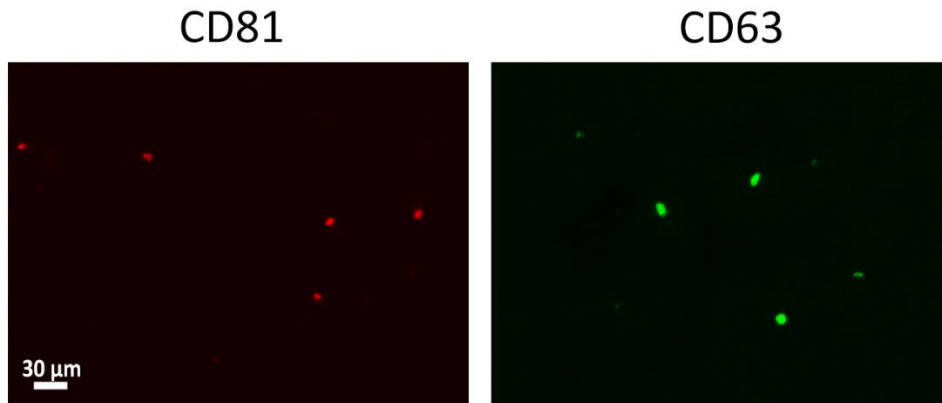


Figure S12. Microscopic images of EV surface markers (left: CD81, right: CD63) marked by immunofluorescence antibodies.

Supplementary Note 11. Optimization of the Fabrication on 96-Well Plates

The incubation time of cell supernatant was optimized. The EV capture efficiency was characterized using confocal microscope. The incubation time had few effect on the average fluorescence intensity.

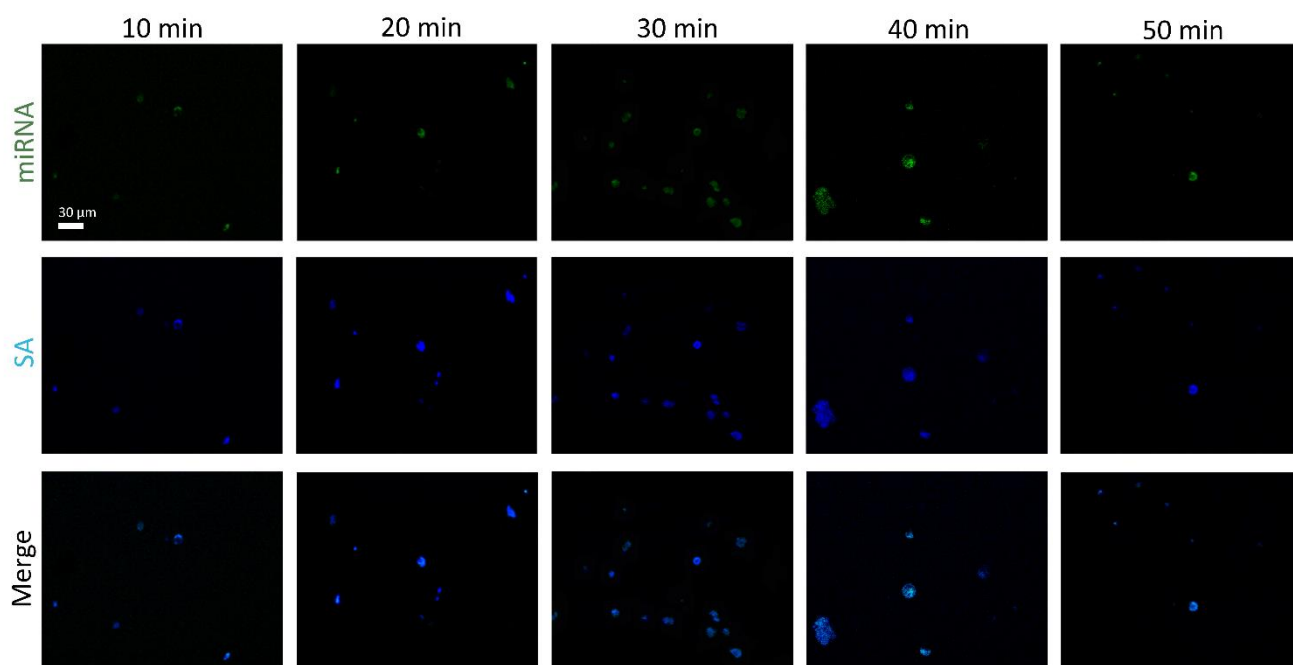


Figure S13. Microscopic images of EVs derived from HeLa cells (200 μ L HeLa supernatant was added to each well and incubated for different time, with laser irradiation for 30 min, standing for 30 min before microscopic imaging) (scale bar: 30 μ m).

Supplementary Note 12. Photothermal Effect of GNP@PDA-NPs

To demonstrate the ability of GNP@PDA-NPs to cause localized EV membrane rupture under laser irradiation, the photo thermal effect of the GNPs was evaluated first (Figure S11a). The temperature distribution of GNPs under laser irradiation can be calculated according to Mie's theory.² The intensity of the absorbance cross section $\sigma_{\text{abs}} = k \text{Im}\alpha$, where k is the wave vector of the incident light ($k = 2\pi/\lambda = \omega/c$), and α is the polarizability of GNP:

$$\alpha(\omega) = 4\pi R^3 \frac{\varepsilon_{\text{Au}} - \varepsilon_m}{\varepsilon_{\text{Au}} + 2\varepsilon_m} \quad (1)$$

where R is the radius of GNP, ε_{Au} is the dielectric constant of GNP, and ε_m is the dielectric constant of the surrounding environment. Thus the energy per volume produced by GNP could be expressed by the following equation:

$$Q = I\sigma_{\text{abs}} \quad (3)$$

where Q is heat quantity and I is the light intensity. By combining the equation (2) and equation (3), the heat could be calculated by:

$$Q = \frac{\omega}{8\pi} \left| \frac{3\varepsilon_m}{\varepsilon_{\text{Au}} + 2\varepsilon_m} \right|^2 \text{Im}\varepsilon_{\text{Au}} \frac{8\pi I}{c\sqrt{\varepsilon_m}} \quad (4)$$

The temperature distribution around the GNP could be described by the following equation:³

$$\rho(r)C(r) \frac{\partial T(r,t)}{\partial t} = \nabla K(r) \nabla T(r,t) + Q(r,t) \quad (5)$$

where ρ is the density of the environment, C is the heat capacity, K is the thermal conductivity, and r is the distance. When $r > R$:

$$\Delta T(r, \infty) = \frac{V_{\text{Au}} Q}{4\pi K r} \quad (6)$$

Due to the high conductivity of GNP, the whole particle reaches the highest temperature ($r = R$):

$$\Delta T_{\max}(I) = \frac{R^2 \omega}{24K\pi} \left| \frac{3\varepsilon_m}{\varepsilon_{Au} + 2\varepsilon_m} \right|^2 \text{Im} \varepsilon_{Au} \frac{8\pi I}{c\sqrt{\varepsilon_m}} \quad (7)$$

Thus $\Delta T \propto R^2$. Considering a GNP of 60 nm in water at 37 °C, the temperature of GNP under 4×10^3 W/cm² light (680 nm) is ~50 °C. In addition of GNPs, PDA is also able to absorb light owing to the aromatic rings and functional groups of amino and hydroxyl. The melanin-like PDA layer could efficiently convert light into heat, causing photothermal effect.⁴⁻⁵ In this work, typical TEM images revealed that the thickness of the PDA shell of GNP@PDA-NPs was around 5 nm (Figure 2e). Therefore, the concentration of PDA in the as-prepared solution of GNP@PDA-NPs is calculated to be ~0.6 µg/mL. According to the absorbance property of PDA,⁵ the temperature change caused by PDA over a period of 30 min is ~40 °C. By combining the photothermal effect of both GNPs and PDA layer, the temperature of GNP@PDA-NPs under 4×10^3 W/cm² light (680 nm) is ~90 °C, which is enough to improve EV membrane permeability.

To demonstrate the local membrane rupture was induced by the photothermal effect of GNP@PDA-NPs, control experiment of the EVs treated with 680 nm laser irradiation was performed. As shown in Figure S11b, the cell supernatant (200 µL) was treated by laser irradiation (688 nm) for 30 min, and then the supernatant was added into each well of the 96-well plates (modified by EV detection surface) for 30 min before microscopic imaging. From confocal fluorescent images, the green channel intensity of the individual EVs was much lower than EVs treated with GNP@PDA-NPs, which confirmed that the EV membrane rupture was induced by the photothermal effect of GNP@PDA-NPs under the laser irradiation.

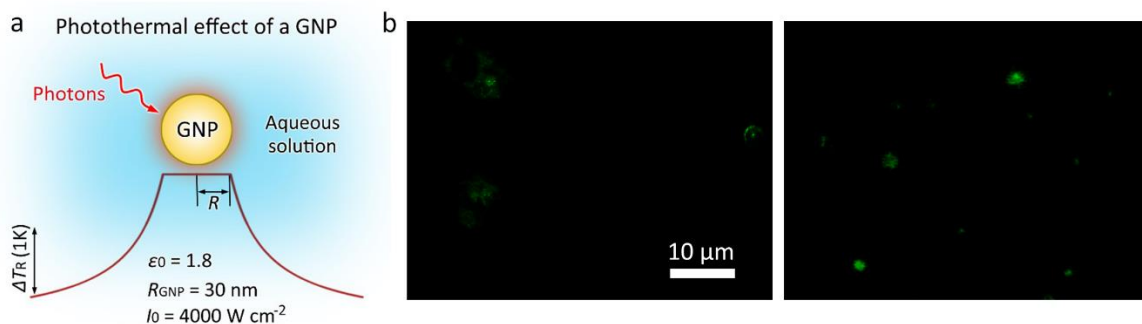


Figure S14. a) Gold particle photothermal effect diagram. b) Microscopic images of EVs derived from HeLa cells (200 μ L HeLa supernatant was treated with laser irradiation without (left) or with GNP@PDA-NPs (right) for 30 min before microscopic imaging) (scale bar: 30 μ m).

Supplementary Note 13. Fluorescence Distribution of the EVs with Different Sizes

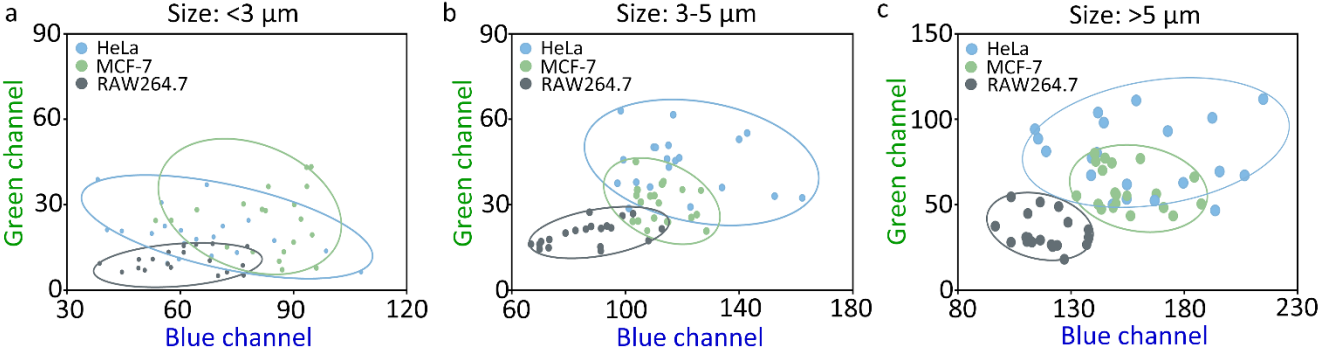


Figure S15. Blue/green channel distribution of the EVs of different sizes from different cells (60 EVs for each cell type, 20 EVs for each size).

Supplementary Note 14. Size Distribution of EVs Derived from Cells Treated with Drugs

The overall size distribution of EVs derived from HeLa cells treated with different drugs showed that the percentage of EVs with diameters larger than 5 μm decreased after drug treatment.

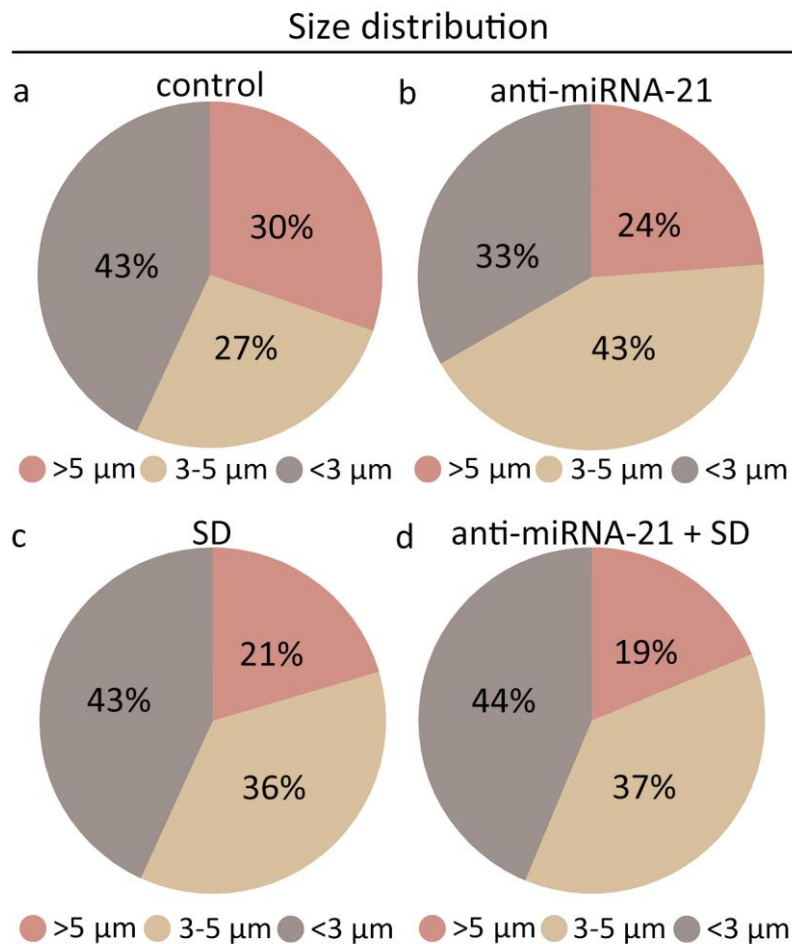


Figure S16. Pie charts showing the average size distribution of EVs derived from HeLa cells treated with a) control, b) anti-miRNA-21 (200 nM), c) SD (60 mU), d) anti-miRNA-21 (200 nM) + SD (60 mU).

Supplementary Note 15. Size Distribution of the EVs from Serum Samples

The size distribution of the EVs from serum samples showed that the percentage of EVs with diameters larger than 5 μ m was much higher in HCC samples.

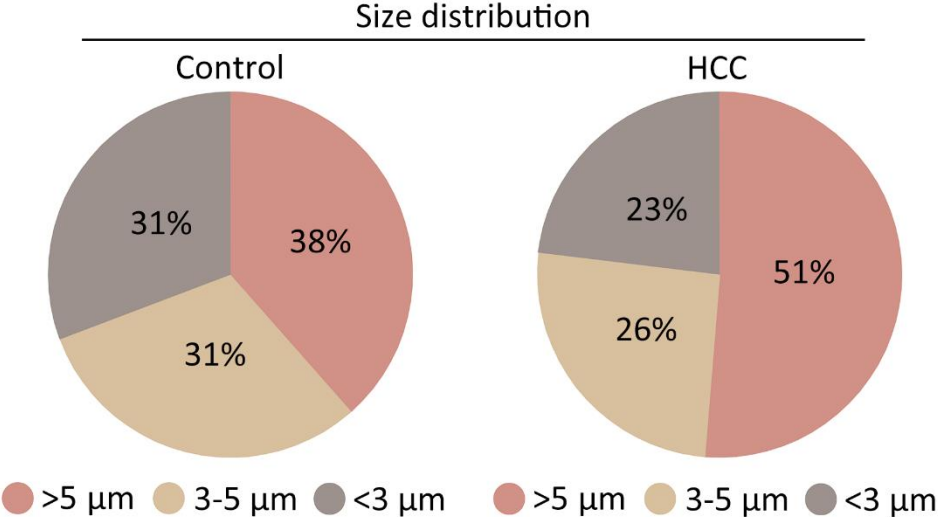


Figure S17. Pie charts showing the average size distribution of EVs in serum samples taken from healthy controls and HCC patients.

References

1. W. Haiss, N. T. K. Thanh, J. Aveyard, D. G. Fernig, *Anal. Chem.* **2007**, *79*, 4215-4221.
2. G. Mie, *Ann. Phys.* **1908**, *330*, 377.
3. A. O. Govorove, H. H. Richardson, *Nanotoday.* **2007**, *2*, 30.
4. Y. Liu , K. Ai , J. Liu , M. Deng , Y. He , L. Lu, *Adv. Mater.* **2013**, *25*, 1353.
5. R. Lv, P. Yang, G. Chen, S.Gai, J. Xu, P. N. Prasad, *Sci. Rep.* **2017**, *7*, 13562.